Magma mixing and metasomatic reaction in silicate–carbonate liquids at the Kruidfontein carbonatitic volcanic complex, Transvaal

L.B. Clarke and M.J. Le Bas

Department of Geology, University of Leicester, LE1 7RH, UK

Abstract

The Kruidfontein volcanic complex is a Proterozoic collapsed carbonatitic caldera structure, the inner caldera of which is filled with carbonatitic bedded volcaniclastic rocks cut by carbonatite dykes, and the outer with bedded silicate tuffs. As well as numerous fragments of phonolitic pumice in the silicate tuffs, there are unusual banded fragments composed of alternating silicate and carbonate compositions which appear to have been originally glasses, and which give evidence for mechanical mixing of magmas which may originally have been magmas separated by liquid immiscibility. The fragments have also been strongly fenitized with the introduction of K and the replacement of Al by Fe.

Keywords: carbonatite, Kruidfontein, South Africa, magma mixing, metasomatic reaction.

Introduction

The circular structure at Kruidfontein, some 100 km NW of Johannesburg, was shown to be the remnants of a carbonatitic volcanic complex by Verwoerd (1967). The structure is typical of many carbonatite complexes and comparable with the Miocene carbonatitic volcano at Kisingiri in western Kenya (Le Bas, 1977). The Kruidfontein complex forms part of a Proterozoic, strongly alkaline, petrographic province which also includes the carbonatitic complexes of Nooitgedacht (Gelukshoek), Spitskop, Goudini (Ystervarkkop), Bulhoek-Tweerivier and Glenover (Verwoerd, 1967). In most of these complexes, pyroxenites, ijolites, nephelinites, phonolites and syenites variously occur. Despite their age, the level of erosion at Kruidfontein, Goudini and several other complexes has not entirely removed the extrusive products of volcanism, whereas at others such as Nooitgedacht and Spitskop, erosion is down to the subvolcanic and intrusive level of former magmatic activity.

Bedded tuffs are preserved at Kruidfontein owing to caldera collapse which occurred there, with the result that tuffs sank below the former surface level of the surrounding banded ironstones, shales and dolomites of the Transvaal Sequence which formed the basement on which the former volcanic edifice rested. Drilling has shown that at least 400 metres of bedded tuffs are preserved in the central area of subsidence. The diameter of the ring fracture is 4 km, and the mechanism of the collapse allowed a central portion 2 km in diameter to sink lower into the basement than the one kilometre wide outer annular ring. Thus at the present day at Kruidfontein is seen a one kilometre-wide outer ring of pyroclastic bedded silicate tuffs enclosing a central block of mainly carbonatitic bedded tuffs (Fig. 1). The silicate tuffs represent the earliest recorded extrusive products from the Kruidfontein carbonatitic volcano. The tuffs comprise both welded and unwelded types, and breccias are interbedded with the tuffs. Within these rocks are widespread phonolitic and syenitic clasts, but some horizons which are darker appear to be more basic in composition. However, the superimposed fenitization and subsequent fluorite mineralization has rendered many of the rocks difficult to identify. Primary mineralogy is rarely preserved but characteristic textures are often still identifiable. In the outer zone and shown on Fig. 1, there are slices, probably fault-bounded, of basement penetrating the silicate tuffs. The presence of such slices suggests the proximity of the basement underneath, as would be expected if the silicate tuffs were erupted early in the history of the volcano.

Mineralogical Magazine, March 1990, Vol. 54, pp. 45–56

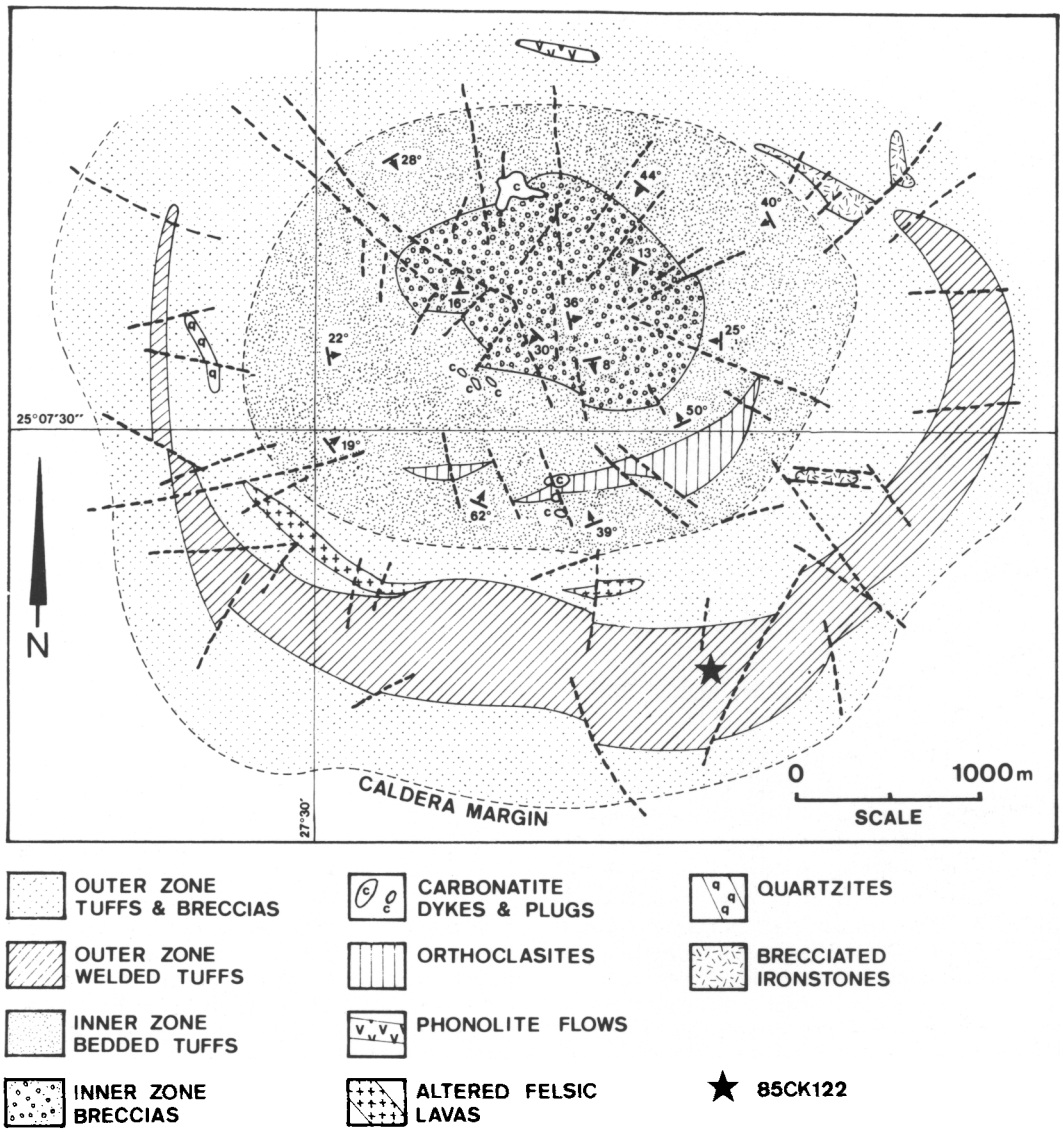

FIG. 1. General map of the Kruidfontein carbonatitic and caldera-collapse volcanic complex showing location (starred) of the sample analysed (85CK122). The outer zone of the caldera is comprised dominantly of silicate tuffs with phonolitic and syenitic clasts; the inner zone is comprised dominantly of carbonatitic tuffs cut by carbonatite dykes.

This paper investigates the geochemistry of some of the phonolitic pumices and of the material in the banded silicate–carbonate fragments in the silicate tuffs. The latter are related to a possible mechanism of magma mixing. It is proposed that silicate and carbonate magmas which co-existed in the sub-caldera magma chamber at Kruidfontein, mixed at the time of explosive eruption to produce clasts of interbanded silicate and carbonate glasses which were subsequently metasomatized. The more abundant phonolitic pumice fragments were also K- and Fe-metasomatized.

Phonolitic pumice fragments

In the bedded silicate tuffs of the outer zone at Fonteinkop, on the south side of the Kruidfontein complex, there occur broken pieces of

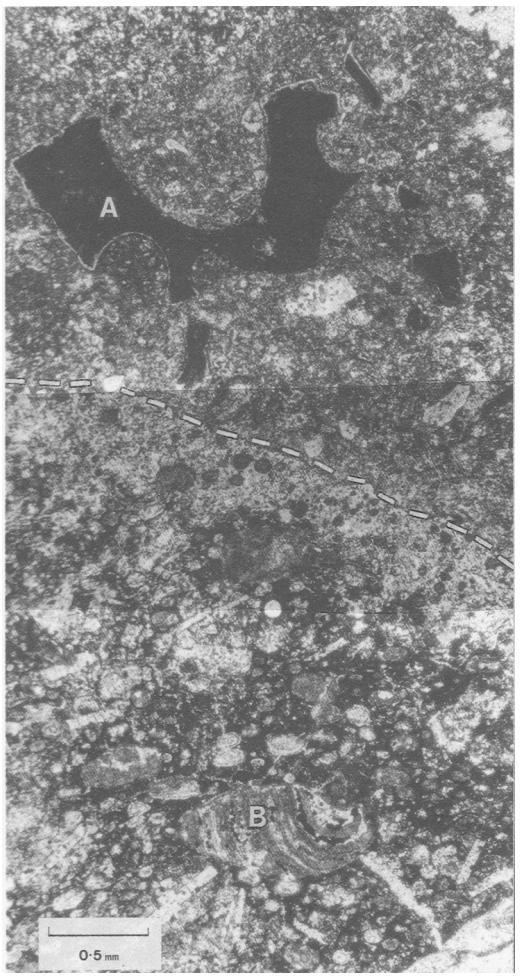

FIG. 2. Montage of three photomicrographs of the lapilli tuff 85CK122 showing at the top (A) one of the fragments of pumice analysed surrounded by smaller fragments and all with whitish rims (K-rich). The matrix includes calcite, opaque phases, chlorite and fluorite. The white dashed line across the middle marks the boundary of a clast which occupies the lower portion of the photograph. This clast has a wide pale coloured margin and darker interior within which is the banded glass fragment (B) described, analysed and discussed later in this paper.

nonporphyritic pumice which under the microscope appear isotropic and evidently were glassy, although they are now slightly devitrified and show a barely perceptible fine felsitic texture. The fragments are only several millimetres across. Some are strongly flattened, others preserve the original round vesicular structure; all gradations from strong deformation to completely undeformed are present (Figs 2, 3, 4). It is deduced that the fragments represent chilled vesiculated lava that was being erupted from the Kruidfontein volcano. Other fragments in the tuff include coarsely crystalline calcitic clasts interpreted to be fragments of sovitic carbonatite, some of them with fluorite replacing the calcite. Thin albite veinlets (Ab_{99} by microprobe analysis) traverse the pumice clasts and matrix.

Microprobe analyses of the pumice fragments (Table 1) were made on a JOEL JXA-8600S electron microprobe analyser in the Geology Department at the University of Leicester under wavelength-dispersive conditions at 15kV and 3nA probe current and using ZAF correction procedures. The iron is reported in Table 1 as Fe_2O_3 so that the figures are more easily compared with those in Table 2. The analyses demonstrate that the fragments although formerly glass are no longer uniform in composition, but that they vary according to distance from the surfaces of the fragment. Of their very nature, glassy pumice fragments derived from the explosive eruption of lava should be uniform in chemical composition, or almost so, throughout the fragment. Thus any chemical zonation was fairly certainly produced after emplacement in the tuffs.

The microprobe analytical traverses across the pumice fragments showed that the most marked feature is the increase in K_2O in the pale margin all round each fragment whether deformed (Figs 3F and 4) or not (Figs 2A and 3A). The uniform profile of K_2O across all the fragments analysed is shown in Fig. 5. The detailed profile along traverse H in Fig. 3 is shown in Figs 6*a* and 6*b*, and it can be seen that the pairs Na_2O and K_2O, Al_2O_3 and Fe_2O_3 both behave antipathetically. That K replaces Na is implied by the simple relation shown in Fig. 7, and can be shown by determining the sum of the molecular proportions for Na and K. The sum should remain constant. The mean sum and standard deviation of the oxide weight percentages divided by the respective Na_2O and K_2O molecular weights for the seven analyses in traverse H are 0.180 and 0.004. Since the standard deviation figure is less than the figure that could be analytically detected, it would seem that K substituted for Na on an atom for atom basis.

Likewise, taking all the analytical data for Al_2O_3 and Fe_2O_3 given in Table 1, the mean sum of the molecular proportions for the 42 analyses is 0.1849 and the standard deviation is 0.0039, again indicating atom for atom replacement of Al by Fe. Fig. 8 illustrates the simplicity of this replacement. The overall chemical variation is

Table 1. Microprobe analyses from traverses across pumice fragments in lapilli tuff 85CK122.

	A1	A2	A3	A4	A5	A6	A7	B1	B2	B3
SiO_2	61.3	59.6	57.1	57.6	59.1	58.1	56.6	58.9	58.7	61.6
Al_2O_3	16.8	14.3	10.0	10.3	13.3	11.2	9.5	12.3	12.2	17.2
Fe_2O_3	2.1	6.5	14.2	14.3	8.9	11.3	14.9	10.6	10.5	2.4
CaO	0.1	0.3	0.8	0.7	0.4	0.6	0.7	0.5	0.6	0.1
Na_2O	0.7	2.7	6.1	6.0	3.5	5.0	6.3	4.6	4.4	0.7
K_2O	15.0	12.6	8.2	8.5	11.5	9.8	8.0	10.3	10.1	15.0
BaO	1.4	1.3	0.8	0.7	1.0	0.8	0.6	1.1	1.1	1.7
Total	97.4	97.3	97.2	98.1	97.7	96.8	96.6	98.3	97.6	98.7

	C1	C2	C3	C4	C5	C6	D1	D2	D3	D4
SiO_2	62.4	58.6	59.0	60.5	57.2	61.6	60.7	57.1	59.0	60.3
Al_2O_3	17.3	11.3	13.1	14.0	11.8	16.2	17.2	10.5	11.8	15.2
Fe_2O_3	1.7	11.7	9.5	6.9	12.5	4.2	2.6	13.6	12.0	6.1
CaO	0.0	0.6	0.5	0.4	0.5	0.2	0.3	0.7	0.6	0.5
Na_2O	0.6	5.0	3.6	2.9	4.5	1.8	0.4	5.8	5.2	2.1
K_2O	15.4	10.0	11.1	12.4	10.0	13.9	15.3	6.8	9.8	13.1
BaO	1.6	0.8	0.8	0.9	0.6	1.6	1.0	0.8	0.8	1.0
Total	99.0	98.0	97.6	98.0	97.1	99.5	97.5	97.3	99.2	98.3

	E1	E2	E3	E4	E5	E6	F1	F2	F3	F4	F5
SiO_2	61.2	57.9	60.6	57.2	58.1	62.2	59.3	59.2	58.9	60.7	59.6
Al_2O_3	16.8	10.9	14.1	9.2	11.9	17.3	13.4	14.2	12.6	16.7	13.4
Fe_2O_3	3.2	13.3	7.5	15.0	11.0	1.5	8.5	8.3	11.3	3.8	8.7
CaO	0.1	0.6	0.4	0.9	1.3	0.1	1.0	0.3	0.5	0.5	0.4
Na_2O	1.2	5.6	3.1	6.6	4.4	0.7	3.4	3.0	4.7	1.1	3.6
K_2O	14.6	9.0	12.3	7.5	10.3	15.5	11.5	11.9	10.5	14.5	11.5
BaO	1.8	0.6	0.8	0.6	0.8	1.6	0.9	0.9	0.8	1.1	0.9
Total	98.9	97.9	98.8	97.0	97.8	99.0	98.0	97.8	99.3	98.4	98.1

	G1	G2	G3	G4	H1	H2	H3	H4	H5	H6	H7
SiO_2	61.7	58.4	58.9	63.0	61.8	59.1	58.6	58.9	59.6	60.4	62.2
Al_2O_3	16.0	11.0	11.8	17.4	16.1	11.9	11.3	12.7	13.1	13.8	17.6
Fe_2O_3	4.5	12.7	10.9	1.5	3.5	11.1	12.4	9.3	9.0	7.4	1.6
CaO	0.3	0.6	0.5	0.3	0.2	0.6	0.7	1.8	0.5	0.5	0.1
Na_2O	1.8	5.4	4.5	0.6	1.3	4.5	5.3	3.9	3.8	3.1	0.3
K_2O	14.0	9.4	10.4	15.8	14.8	10.2	9.5	10.9	11.5	12.1	15.9
BaO	1.2	0.8	0.7	1.1	0.5	0.8	0.6	0.9	0.9	0.8	1.1
Total	99.5	98.3	97.7	99.7	98.2	98.2	98.4	98.4	98.4	98.1	97.9

shown on Fig. 9, where the oxide values are plotted against Al_2O_3. All show simple rectilinear variations except CaO and BaO. Seven of the 42 CaO points plot in Fig. 9 above the remainder which is interpreted to represent minor calcite or fluorite veining (but which is not apparent in thin section). BaO also shows some scatter. Probe-based counting statistics indicate a 16% relative error for BaO at the 95% confidence limit (i.e. *c.* ± 0.1), and thus at Al_2O_3 values less than 15% the apparent scatter in BaO is in fact not significant. But at higher Al_2O_3 values, the scatter is real. When BaO is plotted against K_2O (Fig. 10), there is again no significant scatter at low K_2O values, but for $K_2O > 12\%$ the wide spread of BaO figures, ten times greater than the error figure, indicates that the Ba behaved independently of the K, despite the fact that the BaO also is clearly related to distance from the broken surface of the pumice fragments. It would therefore seem that Ba was introduced after the deposition of the pumice fragments in the tuffs and either before or after the atom for atom replacements described above. Most likely, the Ba was introduced at the same time as the fluorite mineralization which is locally developed in the rock.

The values of SiO_2, Al_2O_3 and Fe_2O_3 at the broken surface of the fragments as well as at the surface of the vesicles are approximately those for a phonolite. But in the glassy interior of the pumice fragments away from the broken and vesicle surfaces, the Al_2O_3 reduces as the Fe_2O_3 increases, and reaches a maximum furthest from the surfaces indicative of metasomatic exchange occurring right through the fragments.

That these pumices originally had phonolitic compositions may be ascertained by comparing them with the phonolites and syenites of the Kruidfontein complex. Table 2 gives the compositions of average phonolites for comparison with the Kruidfontein rocks including syenitic clasts from the same tuff. CIPW norms of analyses 3

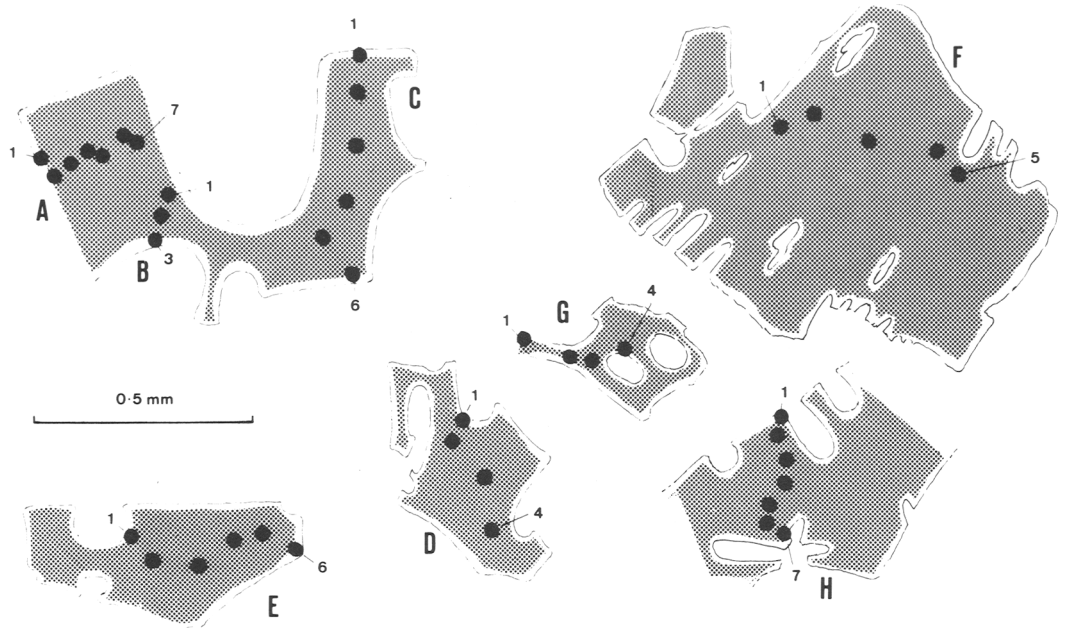

FIG. 3. The six pumice clasts analysed. The numbered spots indicate the sequential positions of microprobe analyses along traverses A to H given in Table 1. Some of the phonolitic pumice fragments show deformation after vesiculation; some are undeformed. The white rim around each fragment corresponds to the most strongly K-metasomatized portions, a process which occurred after incorporation in the tuff.

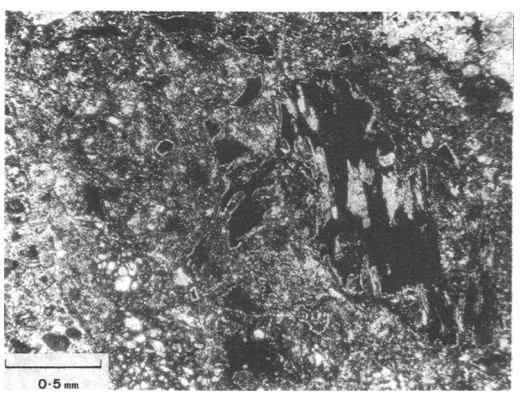

FIG. 4. A pumice fragment showing the deformation by flow before incorporation in the tuff and the white rim which formed after incorporation in the tuff. Most of the larger patches of white matrix material are calcite with feldspar in the finer grained parts.

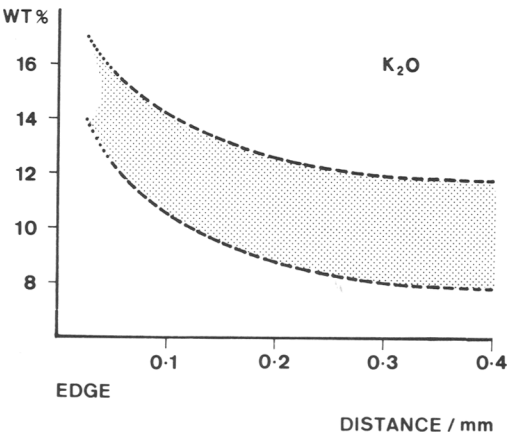

FIG. 5. Profile of K_2O across the pumice clasts in tuff 85CK122 using all the data given in Table 1.

and 4 in Table 2 show they are nepheline normative and no. 3 is acmite normative. Both have about 70% normative alkali feldspar and correspond to phonolite. Norms of the last four analyses in Table 2 do not give sensible compositions owing to the Al–Fe and Na–K substitutions. However they are all broadly phonolitic, if the Na–K and Al–Fe substitutions are taken into account. On the Total Alkali–Silica classification (Le Bas *et al.*, 1986) all but one (no. 4) of the analyses listed lie in the phonolite or tephriphonolite fields. No. 4 lies just in the trachyte field of TAS.

Table 2. Phonolitic and related compositions, calculated 100% anhydrous.

	1	2	3	4	5	6	7	8
SiO_2	57.4	55.4	55.6	60.8	51.7	59.1	63.3	53.1
TiO_2	0.6	0.5	1.7	0.2	0.0	–	–	1.3
Al_2O_3	19.5	20.8	14.1	16.8	0.5	10.6	16.5	15.9
$Fe_2O_3^T$	5.1	5.2	12.8	7.3	29.4	14.7	3.5	12.0
MnO	0.2	0.2	0.5	0.2	1.7	–	–	0.3
MgO	1.1	0.5	1.7	1.3	0.8	–	–	0.4
CaO	2.8	2.9	2.9	1.7	3.3	0.7	0.2	3.3
Na_2O	8.0	9.1	5.5	7.8	12.4	6.2	1.3	0.3
K_2O	5.4	5.5	5.2	3.7	0.1	8.8	15.2	13.5

$Fe_2O_3^T$ = Total Fe determined

1. Average world phonolite (Le Maitre, 1976).
2. Average East African phonolite (Le Bas, 1977).
3. Phonolite dyke (85CK123), S. Kruidfontein.
4. Phonolitic fragment F12 in lapilli tuff (85CK122), S. Kruidfontein.
5. Band 8, felsic silicate in banded fragment (85CK122), S. Kruidfontein.
6. Centre of pumice fragment A4 in lapilli tuff (85CK122), S. Kruidfontein.
7. Edge of pumice fragment H1 in lapilli tuff (85CK122), S. Kruidfontein.
8. K-feldspathized phonolite dyke (86CK80), S. Kruidfontein.

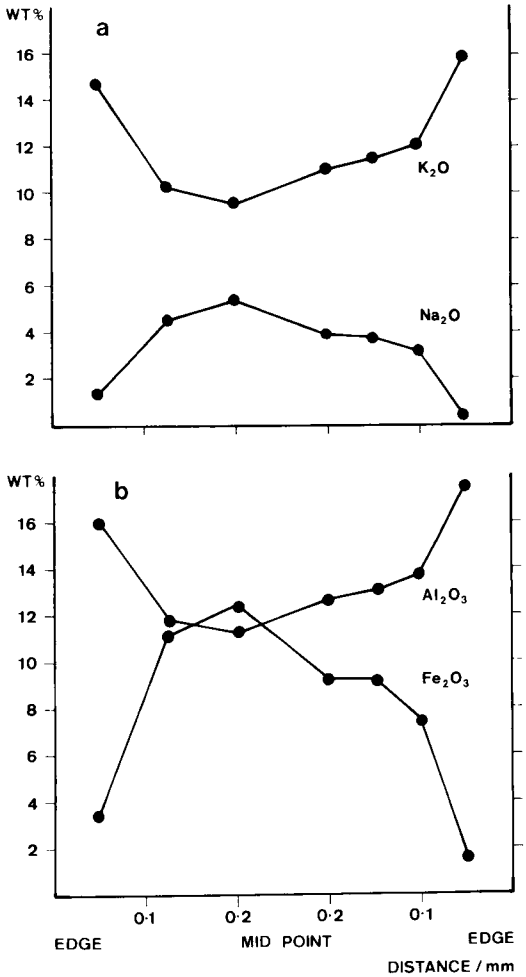

FIG. 6. Profiles along traverse H of glassy phonolitic pumice illustrated in Fig. 3: (*a*) antipathetic relation of K_2O *v.* Na_2O, with K_2O replacing Na_2O; (*b*) antipathetic relation of Al_2O_3 *v.* Fe_2O_3 with Fe_2O_3 replacing Al_2O_3 increasingly away from the edge of the clast.

The covariance of the Al–Fe and Na–K substitutions is taken to indicate that they took place simultaneously. The metasomatic movement of K is one of the most common fenitizing processes associated with carbonatites, and commonly accompanies the formation of orthoclasites with 14% or more K_2O (Le Bas, 1987) a process which is widespread in the southern half of the Kruidfontein complex. The composition of the white rims around the pumice fragments is closely similar to the composition of orthoclasites which are composed almost wholly of high-K feldspars plus some iron oxides and which occur in fenites adjacent to the coarse calcite carbonatites seen in many complexes. Orthoclasites are particularly common in the rocks capping subvolcanic carbonatite intrusions (Le Bas, 1987).

Therefore the introduction of K to the pumice is most likely the product of fenitizing solutions emanating from crystallizing carbonatite magma. It has been argued above that the K and the Fe metasomatic migrations must be related, but the process which permits Fe, but apparently not K, to penetrate into glasses is not clear. It might be related to the relative ionic sizes of Fe and K ions; the latter are almost twice the diameter of the former.

The introduction of Fe is also poorly understood, particularly as the Fe progressively replaces the Al *into* the centres of the pumice clasts. This replacement is comparable to that of Al by Fe in the lattice of potassium feldspars which has been reported (Coombs, 1954).

Banded glass fragment

In the same silicate tuff with the phonolitic pumice fragments there are also vesicular chloritized lithic clasts which contain banded glass fragments now recrystallized. Also in the tuffs are clasts of fine feldspar-rich rocks, now recrystallized, which microprobe analysis shows were formerly syenites.

The lithic clast containing the banded glass

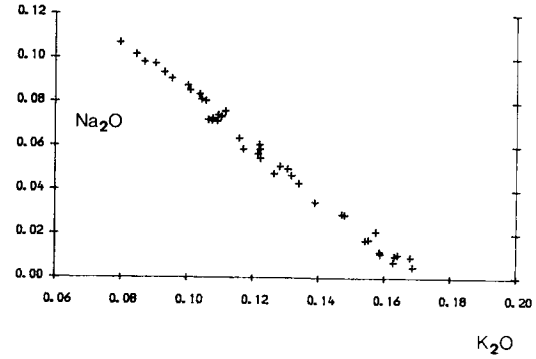

FIG. 7. Molecular proportions K_2O *v.* Na_2O plot of data taken from all transverses given in Table 1. The molecular sum is constant indicating the simple substitution of K for Na.

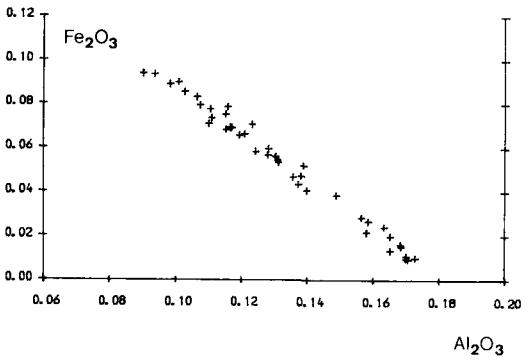

FIG. 8. Molecular proportions Al_2O_3 *v.* Fe_2O_3 plot illustrating the simple substitution of Fe for Al, following the relation Al + Fe = 0.185. The plots shown here and in Fig. 7 indicate that the data are uniform in all the pumice clasts depicted in Fig. 3.

fragment which has been analysed, is composed of opaque material with microphenocrysts of colourless square-ended lath-shaped crystals, now replaced by analcime, and has vesicles filled by a fine aggregate of chlorite, calcite and an opaque phase. The margins of the clast appear to be a fine felsitic intergrowth of alkali feldspar and chlorite. The banded glass fragment was at first mistaken for an unusually large amygdale which did not have the usual circular form, but analysis by microprobe showed it to be a fragment of banded silicate rock which was formerly glassy. The bands in the fragment are lensoid and drawn out in a texture reminiscent of flow-banded rhyolites (Fig. 11).

Thirty-one microprobe analyses were made in a traverse across the bands. They are given in Table 3 and plotted in Fig. 12, except for no. 1

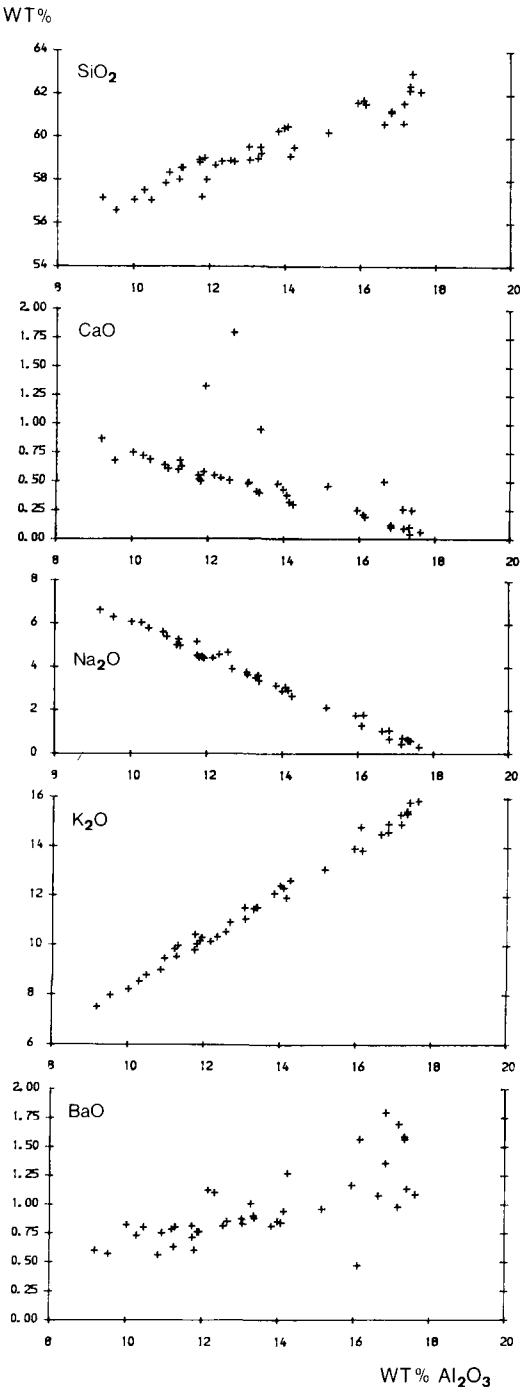

Fig. 9. Overall chemical variation across the pumice clasts shown in Fig. 3. They are plotted against Al_2O_3 and all show rectilinear variation except BaO. The CaO plot shows some points which anomalously lie above the remainder and which are most likely to be produced by minor amounts of calcite or fluorite.

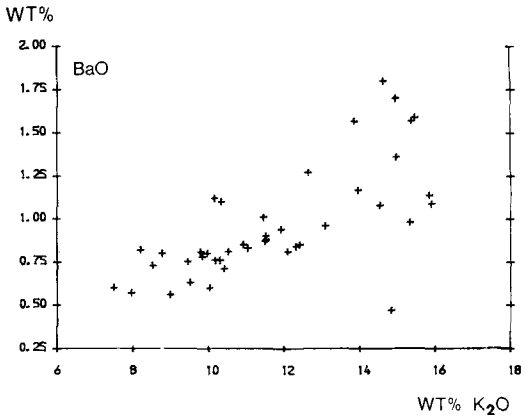

FIG. 10. K_2O *v*. BaO plot showing the poor correlation of the two, which suggests that at the margins of the clasts the introduction of Ba was independent of the K metasomatism.

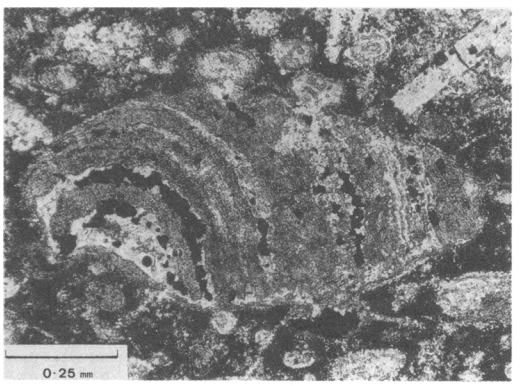

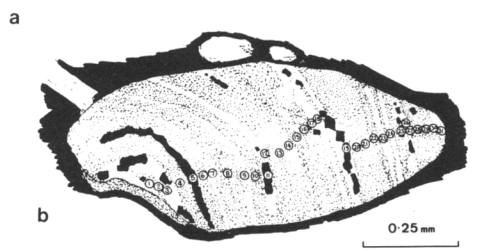

FIG. 11. (*a*) Photomicrograph and (*b*) drawing of the fragment of flow-banded devitrified glass. They show the lensoid nature of the banding, the euhedral cubic crystals of an Fe-opaque phase and the positions of the 31 microprobe analyses given in Table 3, each beam position being as far as possible on an individual band. The same fragment is seen at the bottom of Fig. 2.

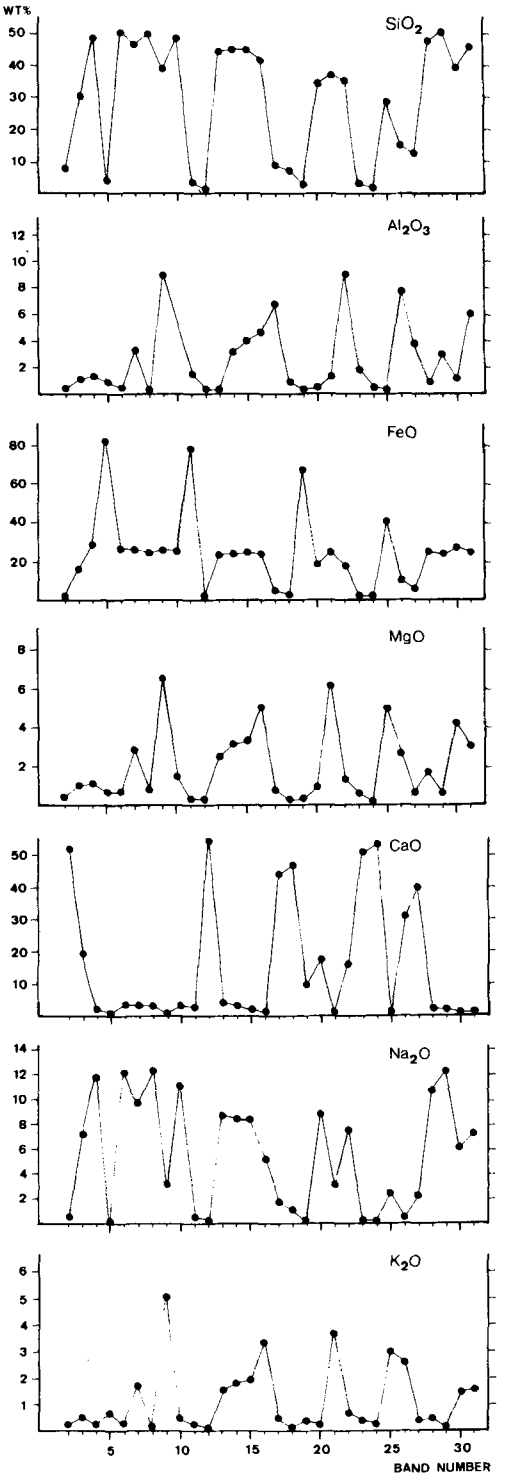

FIG. 12. Traverses for the oxides listed in Table 3 showing the positive and negative correlations.

Table 3. Microprobe analyses of traverse across banded fragment in tuff 85CK122.

Band	SiO_2	TiO_2	Al_2O_3	FeO	MnO	MgO	CaO	Na_2O	K_2O	Total
1	4.2	0.1	1.4	2.9	0.1	0.9	0.1	0.1	0.9	10.6
2	3.8	0.0	0.4	2.4	0.9	0.5	51.6	0.6	0.3	60.6
3	30.3	0.2	1.2	16.7	0.8	1.1	19.2	7.0	0.5	77.1
4	48.3	0.2	1.3	28.8	1.2	1.2	2.0	11.3	0.3	94.7
5	4.1	0.1	1.0	82.0	0.2	0.7	0.3	0.1	0.7	89.2
6	50.2	0.0	0.5	26.7	1.3	0.7	3.4	11.7	0.2	94.6
7	46.3	0.3	3.5	26.6	0.9	2.9	3.5	9.4	1.8	95.2
8	49.4	0.0	0.5	25.2	1.6	0.8	3.1	11.8	0.1	92.5
9	38.7	0.5	9.4	26.5	1.1	6.6	0.6	3.1	5.2	91.7
10	48.4	0.1	1.7	25.7	1.6	1.5	3.4	10.7	0.5	93.6
11	3.4	0.1	0.4	79.2	0.1	0.3	2.6	0.4	0.2	86.9
12	0.9	0.0	0.3	1.2	0.9	0.3	54.1	0.1	0.1	57.8
13	44.2	0.2	3.4	23.9	0.9	2.6	4.8	8.4	1.6	89.7
14	44.5	0.3	4.1	24.8	0.9	3.2	3.5	8.1	1.9	91.2
15	44.5	0.3	4.8	25.8	1.0	3.4	1.9	8.1	2.0	91.7
16	41.2	0.4	7.0	25.0	1.0	5.1	1.3	4.9	3.5	89.5
17	8.6	0.1	1.0	5.6	1.0	0.8	43.6	1.7	0.6	63.1
18	7.2	0.0	0.3	3.3	0.8	0.3	46.8	1.1	0.1	60.0
19	2.8	0.0	0.6	68.1	0.3	0.4	9.9	0.0	0.4	82.6
20	34.0	0.2	1.3	18.8	0.8	0.9	17.1	8.5	0.3	81.8
21	36.5	0.4	9.4	25.9	1.1	6.2	0.8	3.0	3.8	87.1
22	35.0	0.2	2.0	18.8	0.9	1.4	16.1	7.3	0.7	82.5
23	3.1	0.0	0.6	2.5	0.9	0.6	50.6	0.3	0.4	58.9
24	2.0	0.1	0.3	1.3	0.7	0.2	53.0	0.3	0.2	58.1
25	28.4	0.3	8.0	41.0	1.0	5.0	0.9	2.4	3.1	90.2
26	15.6	0.3	4.0	10.5	1.1	2.7	31.2	0.6	2.7	68.8
27	11.4	0.0	1.0	6.6	1.1	0.7	39.9	2.3	0.4	63.4
28	47.5	0.2	2.9	26.1	0.9	1.8	1.5	10.3	0.5	91.8
29	49.9	0.2	1.2	25.6	0.7	0.7	1.6	11.9	0.1	92.0
30	38.9	0.3	7.7	27.8	1.3	4.3	0.9	5.9	1.5	88.6
31	45.7	0.4	5.8	26.1	1.0	3.1	1.0	7.0	1.6	91.8

which was an incomplete analysis but otherwise similar to no. 2. The traverse for SiO_2 suggests that some bands are silicates with 35 to 50% SiO_2 whereas some have little or no SiO_2. Some of the low SiO_2 bands correspond to the bands with high CaO and low Al_2O_3, FeO, MgO and Na_2O, i.e. bands 2, 12, 17, 18, 23 and 24. The totals for these bands average less than 60 and they are carbonate bands as can be confirmed optically. Also corresponding with the low SiO_2 bands are bands with high FeO but low in the remaining oxides (bands 5, 11, 19). In thin section, these high FeO bands can be seen to correspond to bands of opaque cubic minerals and the analyses are close to that for magnetite.

The other bands, all with high SiO_2, appear to divide into those with appreciable MgO, relatively high Na_2O/K_2O ratios and with SiO_2 values in the 30s (e.g. bands 9, 16, 21 and to some extent 25), and those with low Na_2O/K_2O ratios and higher SiO_2 values of 40 or above (e.g. bands 4, 6, 8, 10, 28, 29). But many of the other analyses appear to be mixtures of the four compositions distinguished above. That some of the bands are mixtures is not surprising since the bands are very thin (Fig. 11) and the fine-scaled interbanding means that some of the analyses are likely to be composite because the beam width is broader than some of the bands. Having been glass, the material was also liable to metasomatic alteration, just as were the pumice fragments described above.

In order to calculate the degree of mixing, four analyses were chosen which most closely corresponded to the four compositions distinguished: no. 12—carbonate, no. 5—Fe-oxide (pure magnetite, calculated as FeO, is instead used in the calculation), no. 9—mafic silicate, no. 6—felsic silicate. These four components were used in a least-squares summation PETMIX calculation (Bryan *et al.*, 1969) to determine whether the remaining analyses could be rationalized into simple mixtures of these components. A glance at the analyses listed in Table 3 shows that these are not normal igneous rock analyses since it can be seen that the figures for Al_2O_3 are too low for normal silicate magma compositions and therefore CIPW norms cannot be usefully calculated. The Al_2O_3 figures never exceed 10% and commonly are only 1 or 2%. Similarly the FeO^T reaches figures too high for normal magmatic silicate compositions, but it may be observed that the sum of the Al and Fe oxides produces figures which are within the range of average magmatic compositions, and it has been shown above that in the glassy pumice clasts, Fe can replace Al.

Table 4 lists the components chosen for the PETMIX calculation, the proportions calculated for three of the more strongly mixed bands, and the sum of squares of residuals. Table 5 lists the sum of squares of residuals and the calculated proportions of the components mixed for each of the 30 bands analysed. The weight percentages do not add up to 100 in many cases, partly due to rounding errors, partly due to the original analytical sums not being 100, and in part due to the poor fit of some mixing calculations.

In Table 5, 10 out of the 27 calculations give a sum of least-squares residuals of <0.2 (8 of them <0.1) and all but one are less than 3.0 with only six >1.0. If MnO is combined with FeO, for which it normally substitutes, then 16 of the calculations give residuals <0.2, with 12 <0.1, and the calculations show that MnO is the principal contributor to the high residuals given. The highest residuals are given by the last two analyses of the traverse (nos 30 and 31), and inspection of the calculations shows they are deficient in K_2O, which could be attributed to edge-effect losses (but contrary to those shown for the pumice clasts above). The component which fits least well is the mafic silicate component, and in these cases it is the alkalis, usually K_2O, which give large residuals. In two cases MgO also misfits, and it is clear that the 'ideal' composition for the mafic silicate component is not among those analysed and listed in Table 3. However, allowing for these effects, the calculations indicate that the assumption of mixing the four components chosen is valid.

Table 4. Least squares 'PETMIX' calculations for three bands from the banded fragment.

	Components Mixed: 1	2	3	4	
SiO_2	0.9	0.0	49.4	38.7	1. carbonate
TiO_2	0.0	0.0	0.0	0.5	2. Fe-oxide
Al_2O_3	0.3	0.0	0.5	9.4	3. felsic silicate
FeO	1.2	93.0	25.2	26.5	4. mafic silicate
MnO	0.9	0.0	1.6	1.1	
MgO	0.3	0.0	0.8	6.6	
CaO	54.1	0.0	3.1	0.6	
Na_2O	0.1	0.0	11.8	3.1	
K_2O	0.1	0.0	0.1	5.2	

	Band 2 obs.	est.	Residuals (r)	wt%	s.d.*
SiO_2	3.8	3.80	−0.016	1. 95.11	0.14
TiO_2	0.0	0.02	0.011	2. −0.41	0.10
Al_2O_3	0.4	0.51	0.113	3. 4.20	0.45
FeO	2.4	2.40	0.000	4. 2.20	0.55
MnO	0.9	0.95	0.048		
MgO	0.5	0.53	−0.036	Σr^2 = 0.0277	
CaO	51.6	51.60	−0.001	(0.0254)†	
Na_2O	0.6	0.60	−0.059		
K_2O	0.3	0.27	−0.086		

	Band 14 obs.	est.	Residuals (r)	wt%	s.d.*
SiO_2	44.5	44.47	−0.029	1. 2.65	0.48
TiO_2	0.3	0.20	−0.099	2. −0.66	0.35
Al_2O_3	4.1	4.07	−0.034	3. 58.59	1.55
FeO	24.8	24.80	0.000	4. 40.06	1.93
MnO	0.9	1.40	0.502		
MgO	3.2	3.12	−0.080	Σr^2 = 0.3334	
CaO	3.5	3.49	−0.008	(0.0810)†	
Na_2O	8.1	8.16	0.059		
K_2O	1.9	2.14	0.244		

	Band 22 obs.	est.	residuals (r)	wt%	s.d.*
SiO_2	35.0	34.97	−0.031	1. 26.24	0.46
TiO_2	0.2	0.08	−0.122	2. −0.31	0.33
Al_2O_3	2.0	1.83	−0.167	3. 58.11	1.48
FeO	18.8	18.80	0.000	4. 15.58	1.85
MnO	0.9	1.34	0.437		
MgO	1.4	1.57	0.172	Σr^2 = 0.3064	
CaO	16.1	16.09	−0.007	(0.1154)†	
Na_2O	7.3	7.37	0.066		
K_2O	0.7	0.89	0.194		

* standard deviation
† Σr^2 if Mn is combined with Fe in PETMIX calculation

Table 5. The sums of the least squares residuals (Σr^2) and proportions of the mixtures calculated.

Band	Σr^2	Weight percentages calculated: Carbonate	Fe-oxide	Felsic silicate	Mafic silicate
2	0.028	95	–	4	2
3	0.315	33	–	55	8
4	0.236	–	4	92	7
5	0.055	1	85	–	12
6	0.198	–	1	99	–
7	0.505	2	–	68	33
8	Felsic silicate used in calculation				
9	Mafic silicate used in calculation				
10	0.076	1	–	88	12
11	0.030	5	83	3	5
12	Carbonate used in calculation				
13	0.327	5	–	64	32
14	0.333	3	–	59	40
15	0.437	–	–	55	45
16	0.342	–	–	25	74
17	0.053	80	–	11	7
18	0.257	86	–	12	1
19	0.075	19	71	–	7
20	0.991	28	1	65	5
21	1.507	–	1	1	94
22	0.306	26	–	58	16
23	0.020	94	–	1	4
24	0.083	98	–	2	–
25	1.572	1	23	–	77
26	0.481	57	–	–	44
27	0.031	73	–	17	7
28	1.184	–	1	80	20
29	1.134	–	–	98	3
30	6.141	–	4	29	64
31	2.971	–	–	51	52

Table 6. Nephelinitic and comparable rocks, calculated 100% anhydrous.

	1	2	3	4	5
SiO_2	41.8	44.9	49.7	43.4	42.2
TiO_2	2.7	2.5	3.4	5.0	0.5
Al_2O_3	14.8	14.7	8.1	11.8	10.2
$Fe_2O_3^T$	12.6	13.3	13.0	16.5	28.9
MnO	0.3	0.2	0.2	0.3	1.2
MgO	6.6	4.3	5.8	4.6	7.2
CaO	12.2	9.1	15.4	13.3	0.7
Na_2O	4.9	7.2	1.3	2.9	3.4
K_2O	3.6	2.8	2.4	1.3	5.7
P_2O_5	1.1	0.9	0.4	1.0	–

$Fe_2O_3^T$ = Total Fe determined

1. Average world nephelinite (Le Maitre, 1976).
2. Typical East African nephelinite (RR-585), Kisingiri, (Le Bas, 1987).
3. Altered basic dyke (86CK54), W. Kruidfontein.
4. Altered basic lava (K81-6), N. Kruidfontein, (R.E. Harmer, *pers. comm.*).
5. Band 9, mafic silicate in banded fragment (85CK122), S. Kruidfontein.

Since the flow-banded texture may be taken to indicate that the banding in the former glass was magmatic, and allowing for the Al–Fe substitution and the mobility of the alkalis in this carbonatitic complex, it is deduced that the closest natural composition to the felsic silicate magma is phonolite and the closest natural composition to the mafic silicate magma is nephelinite. Comparative analyses for nephelinitic compositions are given in Table 6 and allowing for the above assumptions, the nephelinite identification finds support. Most are strongly nepheline-normative and plot in or near the foidite field in the Total Alkali–Silica classification (Le Bas *et al.*, 1986), despite the large individual differences in the Fe_2O_3, CaO and K_2O contents stated.

Discussion

The carbonate bands in the banded devitrified fragment are long and sinuous, and apparently sharply bounded. This is as might be expected knowing the very low viscosity (5×10^{-2} poises) of carbonatite magma (Treiman and Schedl, 1983). The possibility that the calcitic bands might not represent former carbonate glass but are carbonated zones of Ca lost from the adjacent mafic silicate bands during devitrification and metasomatism is discounted on textural grounds. The

silicate bands are also much thinner than is normally experienced when looking at flow-banded rhyolites. This may be due to the more alkaline and mafic compositions present, but it could also be due to higher than usual fluorine contents (Dingwall, 1989) which would be in accord with the F-rich nature of the whole Kruidfontein carbonatitic complex (Clarke, 1989).

It is uncertain whether the Fe-oxide bands calculated as magnetite represent a magmatic material or are the result of late-stage solutions, perhaps derived from the metasomatic changes affecting the silicate components and then penetrating along the bands. The possibility of a magnetite-rich magma is not unreal remembering the occurrence of such a magma at El Laco in Chile described by Haggerty (1970), and more recently Forster (1989) has described volcanogenic magnetitite magma at Chador Malu in central Iran which is said to be related to a highly alkaline carbonatite magma. In the natrocarbonatite volcano of Oldoinyo Lengai in Northern Tanzania, Dawson *et al.* (1989) report droplets of a K,Fe-rich sulphide set in a sodium-carbonate-rich groundmass within lapilli, which could be interpreted as indicating an Fe-rich immiscible phase, but the antipathetic relation of K and Fe (Table 3 and Fig. 6) does not support the presence of such a phase at Kruidfontein. Instead, it is considered that the frequency of late-stage iron-rich solutions in carbonatitic complexes (Le Bas, 1987; Andersen, 1984) makes a late-stage origin more likely. If the Fe bands are late-stage veinlets, this leaves three co-existing magmatic components represented in the banded fragment: two silicate, deduced above to have originally been nephelinite and phonolite, and one carbonate.

It is suggested that the compositions taken for the carbonate and silicate magmas mixed in the proportions listed in Table 5 give a good approximation, allowing for the metasomatic exchanges, of the composition of the carbonate and two silicate magmas originally available for extrusion at the Kruidfontein volcanic centre. The Ca-rich carbonate component is typical of sovitic carbonatites and would match the sovitic clasts observed in the tuff and the sovitic intrusions of the complex. Whether or not the carbonate magma may have carried alkalis as well is not an argument which can be pursued here, but it is not inconceivable that any alkalis which it may have once contained were lost to the adjacent silicate components.

Of the silicate components, most (14) are phonolitic or largely phonolitic with Na_2O averaging about 10% and K_2O usually <1% and often <0.5%, while the nephelinitic component averages 6 to 7% MgO, Na_2O *c.* 3% and K_2O *c.* 4%. This distribution of the alkalis contrasts with that in the pumice fragments, where K_2O rises above 10% and Na_2O decreases to <1%. The pumices were juvenile in the tuff but the banded fragment is enclosed in a larger clast and thus was derived from deeper in the volcano where the controls of alkali metasomatism may have differed. The migration of alkalis during fenitization is still imperfectly understood. The possible migration of alkalis and other components in glasses during alteration is yet another problem. Oxygen isotope analysis shows that large-scale exchange of oxygen takes place during the alteration, particularly hydration, of glass, and therefore at least some exchange of other constituents is to be expected (Carmichael, 1979). The Al–Fe and Na–K exchanges evident at Kruidfontein indicate that Fe and K must have had high activities in the fluids causing the exchange, although they behaved antipathetically.

The assemblage of a single carbonate and two silicate magmatic compositions closely approximates to that found in typical carbonatitic complexes (Heinrich, 1966; Le Bas, 1977, 1987). The preponderance of phonolitic compositions and paucity of nephelinitic compositions, together with the co-existing nature of the one carbonate with the two silicate former glasses, i.e. magmas, quenched together in the banded fragment, could be accounted for by the following petrogenetical scheme.

The general geology of the Kruidfontein volcanic complex indicates that both phonolitic and carbonatitic magmas were available during the caldera collapse stage of evolution of the complex, but that the nephelinitic lavas and dykes, identified only with some difficulty owing to the considerable subsequent alteration, are less common (Clarke, 1989). This suggests that the subvolcanic chamber was largely filled by phonolitic magma with minor amounts of sovitic magma, the two perhaps co-existing as immiscible liquids. If the particular eruption which formed the bedded tuffs described above had been triggered by the intrusion of a pulse of nephelinitic magma, coming from a deeper crustal magma chamber or perhaps directly from the mantle, then the intrusion of hot basic magma could cause explosive eruption of the magmas in the upper chamber. This would result in the eruption of a mixture of phonolitic and carbonatitic melts entrained in each other with further entrainment of streaks of nephelinitic melt.

While buried in the tuff, the fragment was subjected to metasomatic processes associated with fenitization which caused Al to become mobilized

and replaced by Fe, and caused the migration of potassium and exchange of alkalis. The nature of the fenitizing fluids remains uncertain except that they are related to the underlying carbonatite, and it is suggested that the mobility of the Al could be related to the migration of fluoride-bearing solutions through the bedded tuffs. Several episodes of fluorite mineralization are known at Kruidfontein, one producing the massive stratiform fluorite deposit which has been trenched and drilled but not exploited on the western side of the complex.

The banded glassy fragments and the clasts of pumice in the tuffs thus encapsulate the nephelinite–phonolite–carbonatite magmatic history of the Kruidfontein volcanic complex as well as some of the later fenitic events.

References

Andersen, T. (1984) *Lithos*, **17**, 227–45.

Bryan, W. B., Finger, L. W., and Chayes, F. (1969) *Science*, **163**, 926–7.

Carmichael, I. S. E. (1979) Glass and Glassy Rocks. In *Evolution of the Igneous Rocks* (H. S. Yoder, ed.) 233–44. Princeton Univ. Press, New Jersey.

Clarke, L. B. (1989) Ph.D. thesis, University of Leicester.

Coombs, D. S. (1954) *Mineral Mag.* **30**, 409–27.

Dawson, J. B., Smith, J. V. and Steele, I. M. (1989) *J. Geol.* **97**, 365–72.

Dingwall, D. B. (1989) *Am. Mineral.* **74**, 333–8.

Haggerty, S. E. (1970) *Ann. Rept. Dir. Geophys. Lab. Carnegie Inst. Yearb.* **68**, 329–30.

Heinrich, E. Wm. (1966) *The geology of carbonatites*. Rand McNally, Chicago.

Le Bas, M. J. (1977) *Carbonatite-nephelinite volcanism*, Wiley, London.

—— (1987) Nephelinites and carbonatites. In *Alkaline igneous rocks* (J. G. Fitton and B. G. J. Upton, eds), Geol. Soc. Spec. Publ. **30**, 53–83.

—— Le Maitre, R. W., Streckeisen, A. and Zanettin, B. (1986) *J. Petrol.* **27**, 745–50.

Le Maitre, R. W. (1976) Ibid. **17**, 589–637.

Treiman, A. H. and Schedl, A. (1983) *J. Geol.* **91**, 437–47.

Verwoerd, W. J. (1967) *Geol. Surv. S Africa, Handbook*, **6**.

[*Manuscript received 20 June 1989; revised 5 September 1989*]